Waste heat won't make membrane distillation cool: Thermodynamic analysis of cooling and pumping burdens

Desalination 628 (2026) 120039

Contents lists available at ScienceDirect

Desalination

journal homepage: www.elsevier.com/locate/desal

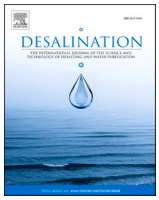

Waste heat won't make membrane distillation cool: Thermodynamic analysis of cooling and pumping burdens

Marco Malaguti [a], Matteo Morciano [b,c], Giulia Viano [d], Andrea Achilli [e], Aamer Ali [d], Cejna Anna Quist-Jensen [a], Alberto Tiraferri [b,f,*]

[a] Center for Membrane Technology, Department of Chemistry and Bioscience, Aalborg University, Fredrik Bajers Vej 7H, 9220, Aalborg East, Denmark
[b] Clean Water Center, Politecnico di Torino, Corso Duca degli Abruzzi 24, 10129, Torino, Italy
[c] Department of Energy (DENERG), Politecnico di Torino, Corso Duca degli Abruzzi 24, 10129, Torino, Italy
[d] AAU Energy, Aalborg University, Pontoppidanstræde 111, 9220, Aalborg East, Denmark
[e] Department of Chemical and Environmental Engineering, University of Arizona, Tucson, AZ, 85721, United States
[f] Department of Environment, Land and Infrastructure Engineering (DIATI), Politecnico di Torino, Corso Duca degli Abruzzi 24, 10129, Torino, Italy

HIGHLIGHTS

- Cooling demand reaches 80–100% of heating in some membrane distillation configurations.
- Cooling availability, not only heat supply, often constrains membrane distillation system feasibility.
- Regardless of the configuration, single pass water recovery does not exceed ~10%.
- Thermodynamic energy requirements differ from actual system consumptions.
- In membrane distillation, "free" heat alone does not guarantee viability.

GRAPHICAL ABSTRACT

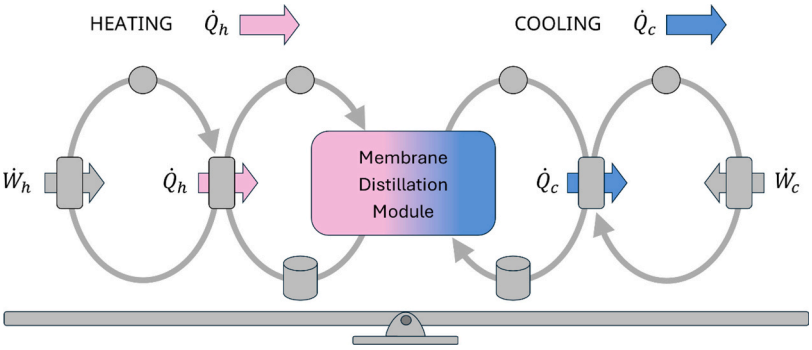

ARTICLE INFO

Keywords:
Desalination
Membrane distillation
Energy analysis
Cooling burden

ABSTRACT

Membrane distillation is promoted as a thermally driven desalination process capable of utilizing low-grade heat, yet its full thermal and hydraulic burdens have not been comprehensively resolved. The cooling burden is often neglected altogether, an assumption rarely met in real applications and especially in severe water stressed regions. This study develops a lumped thermodynamic framework that quantifies heating, cooling, and pumping duties across three representative membrane distillation configurations. Results show that cooling loads can reach the same order of magnitude as heating, up to 80–100% of the thermal input in open-loop feed setups, and remain of comparable magnitude even with internal or external heat recovery. Pumping penalties of 0.2–0.5 kWh/m^3 emerge at typical single-pass water recoveries of only 2–6% and pressure losses of 300 mbar, underscoring the need for joint thermal–hydraulic optimization. The analysis also suggests a techno-economic trade-off: lowering specific energy consumption requires efficient heat utilization, typically achieved through effective system-level integration, large modules, minimization of terminal temperature differences, and internal or external heat recovery solutions; whereas compact designs entail modest capital expenditures but

* Corresponding author at: Clean Water Center, Politecnico di Torino, Corso Duca degli Abruzzi 24, 10129, Torino, Italy.
E-mail address: alberto.tiraferri@polito.it (A. Tiraferri).

https://doi.org/10.1016/j.desal.2026.120039
Received 8 January 2026; Received in revised form 17 February 2026; Accepted 28 February 2026
Available online 7 March 2026

disproportionately high operational expenditures. Finally, a methodology for converting classical energy requirement indicators into actual energy consumption values is presented. The analysis compares different heating and cooling strategies, showing that feasibility relies not only on "free" heat availability, but also on heat sinks effectiveness, optimized heat recovery, and low-resistance module hydraulics.

Nomenclature

MD	Membrane distillation
DCMD	Direct contact membrane distillation
AGMD	Air gap membrane distillation
CapEx	Capital expenditure
OpEx	Operational expenditure
COP	Coefficient of performance (−)
$\dot{Q}$	Heat rate to be provided or extracted (W)
STEC	Specific thermal energy consumption, intended as requirement (kWh/m^3)
SCR	Specific cooling requirement, intended as requirement (kWh/m^3)
$\dot{w}$	Specific energy consumption, intended as consumption (kWh/m^3)
η	Vaporization efficiency (−)
T	Stream temperature (K or °C)
ΔT	Temperature difference between inlet setpoints, $T_{h,in}$ and $T_{c,in}$ (K or °C)
$\Delta T_{h,in}$	Streams temperature difference at the hot inlet, $T_{h,in}$ and $T_{c,out}$ (K or °C)
$\Delta T_{h,out}$	Streams temperature difference at the hot outlet, $T_{h,out}$ and $T_{c,in}$ (K or °C)
ΔT_{HX}	Temperature difference across the heat exchanger (K or °C)
R	Single-pass water recovery (%)
ρ	Density (kg/m^3)
c	Specific heat capacity (J/kg/K)
h_{vap}	Enthalpy of vaporization (J/kg)
τ	Energy conversion efficiency (−)
k	Share of energy to be paid from the OpEx perspective (−)

1. Introduction

Desalination represents a crucial technology to provide access to high-quality water where natural freshwater resources are scarce [1,2]. However, the energy requirements of desalination must be addressed alongside water availability challenges [3,4]. Among available technologies, membrane distillation (MD) stands out for its versatility, modularity, and potential of being powered with low-grade energy sources, valorizing waste heat and theoretically minimizing energy consumption and environmental footprints [5–7]. Although MD represents a promising solution for the desalination of highly saline water streams, its energy demand remains a major barrier to full-scale implementations, especially when compared with mature technologies [8–10]. Moreover, MD energy requirements are frequently reported without accounting for all inputs necessary for actual operation, notably the interplay between thermal and electrical energy [10,11].

Fig. 1A) shows the full energy balance of a generic MD system. Thermal energy drives the separation by generating a temperature difference between the streams (Q_h), while electrical energy is required mostly to circulate streams through the membrane module channels. However, depending on the system configuration, additional cooling duty is required to extract heat from the cold stream (Q_c). This latter burden is rarely quantified in literature, even if its actual contribution has not been unveiled yet, especially in real-scale systems. Most studies neglect cooling altogether, assuming the existence of an unlimited and freely available heat sink, an assumption rarely met in real applications. The challenge is particularly severe in water-stressed regions (e.g., deserts, inland regions), where the need for clean water coincides with limited access to cooling media, such as cold water or ambient air [12,13]. In addition, not only the availability but also the quality of the heat sink is critical for achieving suitable cooling performance, often requiring clean water or dedicated treatment units [14,15]. Even when adequate heat sinks exist, cooling is not cost-free: meeting discharge temperature regulations, ensuring adequate flow rates, operating circulation pumps, all impose an energy and thermodynamic penalty. This reflects the inherent irreversibility of heat rejection, which ultimately manifests as entropy generation [16–18].

Despite the rapid growth in MD research (Fig. 1B), the vast majority of the studies neglect the cooling burden. This research explicitly addresses this gap by quantifying the impact of cooling on the energy requirements of MD systems. A thermodynamic framework for the fair

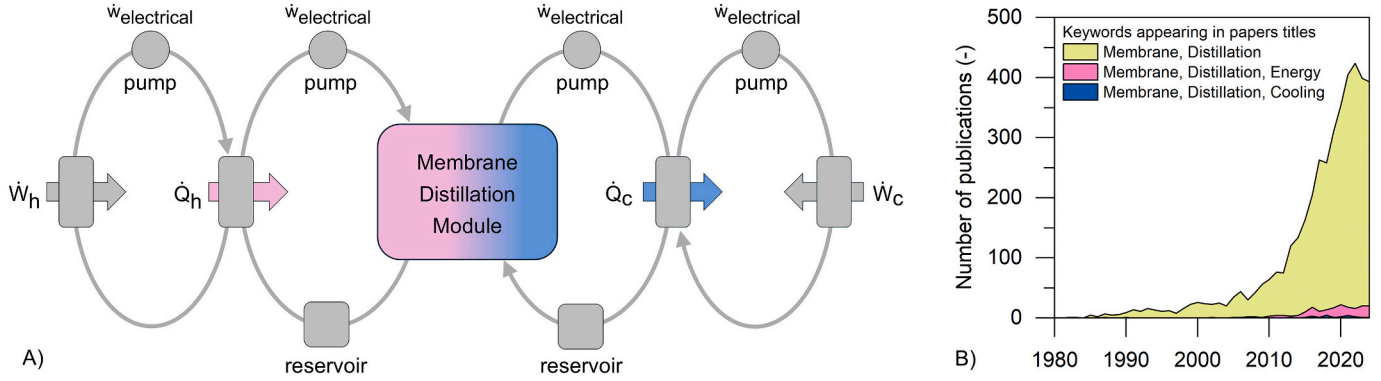

Fig. 1. Introduction to the cooling problem and associated literature gap. A) Schematic energy balance of a generic MD system. Pink and blue arrows indicate heat rate input and extraction, while gray arrows denote the power required to sustain these fluxes. B) Annual number of papers published over the past 45 years (non-cumulative) containing in the title the keywords Membrane Distillation, Membrane Distillation Energy, and Membrane Distillation Cooling. Different colors correspond to different keywords combinations. The data was retrieved from Scopus (August 2025).

assessment of MD energy demands (i.e., heating, cooling, and pumping duties) is developed and applied to three representative MD system designs, also capturing the effects of operational conditions and system configurations. For this purpose, the thermodynamic indicator "specific cooling requirement (SCR)" is newly introduced with the objective of quantifying the minimum amount of heat to be extracted from the cold stream. Furthermore, to pursue a comprehensive energy footprint discussion, energy requirements are converted into energy consumptions by accounting for the technological means used to satisfy them, as well as the availability of free heat sources and heat sinks. This analysis builds upon the authors' previous experimental and modeling work, from proof-of-concept to pilot-scale systems, and reflects the authors' perspective developed through broader considerations of energy systems and their interconnections. In the context of rapid technological development, this viewpoint aims to highlight the importance of merging vertical, technology-specific research with a system-level, energy-oriented perspective, as these approaches are seen as complementary rather than mutually exclusive.

2. Materials and methods

2.1. Reference system configurations

To quantify the impact of cooling on the total energy demand of MD, three representative configurations were selected and schematically illustrated in Fig. 2. The configurations were identified to complement one another and to highlight distinct and relevant trends; however, the same analytical framework can be directly extended to alternative configurations. In a conventional direct contact membrane distillation (DCMD) configuration (panel A), both mass and heat are transferred from the hot feed side to the cold distillate side. Maintaining the desired inlet temperatures requires supplying heat to the feed ($\dot{Q}_h$) and extracting heat from the distillate ($\dot{Q}_c$). In this case, the feed circuit is treated as an open system, with the feed stream passing through the MD module only once and therefore leading to constant inlet salinity. Conversely, the distillate circuit is assumed to be closed, allowing the distillate to accumulate over time [19]. Panel B) considers the same DCMD layout but includes an external heat recovery unit, allowing part of the heat released by the outgoing distillate stream to pre-heat the incoming feed. The feed circuit remains open, and the distillate circuit closed. Lastly, panel C) illustrates an air-gap membrane distillation (AGMD) system with internal heat recovery. The distillate condenses into the air gap, while the saltwater stream circulates through both the feed and cooling channels in a closed circuit. Before re-entering the cold channel, the stream is cooled by extracting a heat rate ($\dot{Q}_c$). In this configuration, make-up water is continuously added to compensate for the vapor losses, ensuring pseudo-steady-state conditions.

2.2. Theoretical thermodynamic analysis

The methodology for evaluating the newly introduced SCR is presented together with the specific thermal energy consumption (STEC). Although STEC is commonly defined in the literature as *specific thermal energy consumption*, it is formally calculated as the thermal energy to be supplied into the system per cubic meter of produced distillate. Therefore, it expresses the heat *required* by the process, rather than the actual energy *consumption* of the system. However, since STEC is firmly established in the literature, its conventional definition is retained here. Nevertheless, STEC should be regarded here as an energy requirement rather than a measure of actual consumption, the latter depending on how such requirement is met and influenced by process configuration, component efficiencies, and irreversibilities.

SCR is intended to be complementary to STEC, quantifying, through an analogous procedure, the amount of energy that must be removed from the distillate stream per cubic meter of produced water. While the specific heating requirement is defined as $STEC = \dot{Q}_h/\dot{m}_d$, the specific cooling requirement is defined as $SCR = \dot{Q}_c/\dot{m}_d$, where $\dot{m}_d$ denotes the flow rate of distillate water flowing across the membrane. A comprehensive thermodynamic framework is developed by building on the pioneering analyses by Christie et al. [20] and Giagnorio et al. [21] who proposed streamlined approaches for evaluating theoretical thermodynamic performance of MD processes.

In detail, this study investigates the effects of (i) vaporization efficiency (η), expressed as the ratio between the heat carried by the vapor flux and the total heat transferred across the membrane (Eq. S1), and (ii) inlet temperature difference between the hot and cold streams ($\Delta T = T_{h,in} - T_{c,in}$) as the main variables within thermodynamically admissible ranges. Seawater is selected as feed stream, while complete salt rejection and production of pure distillate water is assumed. These assumptions directly define the physical properties of the involved streams (density,

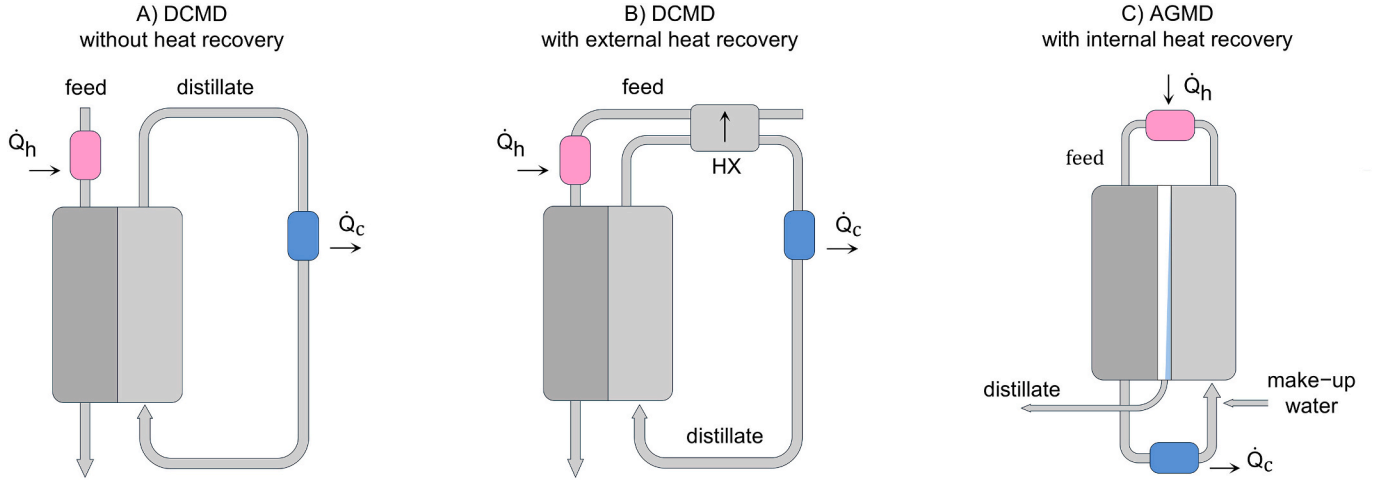

Fig. 2. Schematic representation of the analyzed MD configurations. Pink and blue blocks idealize devices where thermal power is supplied ($\dot{Q}_h$) or extracted ($\dot{Q}_c$), respectively. Panel A) reports a DCMD configuration with open feed and closed distillate circuits. Heat is provided to the feed, while heat is removed from the distillate. Panel B) shows a DCMD system with external heat recovery, where a heat exchanger recovers energy from the distillate stream and transfers it to the feed stream, reducing both heating and cooling requirements. Panel C) displays an AGMD configuration in which heat is recovered within the module (the membrane module acts as a heat exchanger, removing the need for an external device). Here, the saltwater stream circulates through both feed and cooling channels, realizing a closed circuit.

ρ, enthalpy of vaporization, h_{vap}, and specific heat capacity, c), based on temperature- and salinity-dependent correlations reported by Sharqawy et al. [22]. The cold stream inlet temperature is fixed at 20 °C, while both the temperature difference at the hot inlet ($\Delta T_{h,in}$) and the temperature difference across the heat exchanger (ΔT_{HX}) are set to 5 °C. Notice that $\Delta T_{h,in}$ is defined as $T_{h,in} - T_{c,out}$, while $\Delta T_{h,out}$ is defined as $T_{h,out} - T_{c,in}$.

The full theoretical derivation of the lumped-parameter thermodynamic model is provided in the Supplementary Information, along with all the related mathematical definitions and a comprehensive description of the employed variables. The resulting Eqs. (1)–(3) express the cooling and heating requirements for the three different configurations analyzed:

$$SCR_{conf.1} = \frac{h_{vap}}{\eta}\cdot\frac{\Delta T - \Delta T_{h,in}}{\Delta T - \Delta T_{h,out}}, \qquad STEC_{conf.1} = \frac{h_{vap}}{\eta}\cdot\frac{\Delta T}{\Delta T - \Delta T_{h,out}} \tag{1}$$

$$SCR_{conf.2} = \frac{h_{vap}}{\eta}\cdot\frac{\Delta T_{HX}}{\Delta T - \Delta T_{h,out}}, \qquad STEC_{conf.2} = \frac{h_{vap}}{\eta}\cdot\frac{\Delta T_{h,in} + \Delta T_{HX}}{\Delta T - \Delta T_{h,out}} \tag{2}$$

$$SCR_{conf.3} = \frac{h_{vap}}{\eta}\cdot\frac{c_c}{c_h}\cdot\frac{\Delta T_{h,out}}{\Delta T - \Delta T_{h,out}}, \qquad STEC_{conf.3} = \frac{h_{vap}}{\eta}\cdot\frac{\Delta T_{h,in}}{\Delta T - \Delta T_{h,out}} \tag{3}$$

The developed model also enables a quantification of the pumping energy required to circulate water within the MD module per cubic meter of produced water. This contribution depends on the single-pass water recovery (R), which is an output variable of the model defined as the ratio between the produced distillate flow rate and the inlet feed flow rate. Therefore, specific pumping energy can be estimated as $\Delta P/(R \bullet \eta_{pump})$, with the full derivation reported in the Supplementary Information. The pumping energy consumption depends on pump efficiency (η_{pump}), total hydraulic pressure drop along the module (ΔP), and R, the latter depending in turn on η and ΔT.

2.3. Evaluating the role of heat sources and heat sinks

While STEC and SCR quantify the specific energy requirements, they provide no insight into the means used to deliver or extract energy, nor into the nature, cost, or quality of the associated heat sources and sinks. To bridge this gap and move from idealized thermal metrics to real energy consumptions, two auxiliary quantities are introduced: the specific energy consumption for heating, $\dot{w}_h$, and for cooling, $\dot{w}_c$. These quantities are defined in Eqs. (4) and (5), together with their corresponding net values ($\dot{w}_{h,net}$ and $\dot{w}_{c,net}$), which represent the share of energy that must be supplied through paid energy carriers, i.e., the portion that incurs an operational cost.

$$\dot{w}_h = \dot{w}_{h,pump} + \frac{STEC}{\tau_h}, \qquad \dot{w}_{h,net} = k_{h1}\cdot\dot{w}_{h,pump} + k_{h2}\cdot\frac{STEC}{\tau_h} \tag{4}$$

$$\dot{w}_c = \dot{w}_{c,pump} + \frac{SCR}{\tau_c}, \qquad \dot{w}_{c,net} = k_{c1}\cdot\dot{w}_{c,pump} + k_{c2}\cdot\frac{SCR}{\tau_c} \tag{5}$$

The terms $\dot{w}_{h,pump}$ and $\dot{w}_{c,pump}$ express for the auxiliary pumping energy required to circulate technical fluids within the heating and cooling circuits. Note that these pumping contributions differ from those related to circulating water within the MD module. The dimensionless parameters τ_h and τ_c act as conversion factors of heating and cooling systems, linking the thermal energy required at the point of use to the supplied (primary) energy. For direct resistive heating $\tau \approx 1$, while for heat-pump heating systems $\tau \approx$ COP >1 (less primary energy per unit of delivered heat). Conversely, the limiting convention $\tau \to \infty$ is used when heating or cooling can be provided without direct generation or conversion (e.g., freely available waste heat or cooling water), so that the corresponding term in Eqs. (4) and (5) vanishes and only pumping contributions remain. The coefficients k_1 and k_2 (ranging from 0 to 1) identify the paid fraction of energy (from the operational cost perspective). For example, $k_2 = 0$ when the heating requirement is entirely covered by solar thermal energy, while $k_2 = 1$ when the demand must be supplied through paid energy carriers (electricity, gas, or mechanical chillers), and intermediate values for hybrid cases. Pumping energy required for heating and cooling circuits is herein always considered paid energy ($k_1 = 1$).

Cooling differs from heating because energy is required to remove heat from the cold stream and lower its temperature. If freely available cold sources (i.e., ambient air, surface water) are sufficient to reach the target inlet temperature, the cooling cost reduces to the circulation of the technical fluid, i.e., only $\dot{w}_{c,pump}$ remains while $SCR/\tau_c \to 0$. This behavior is similarly appearing when waste heat is employed for fulfilling the heating duty. Five heating options (solar thermal, waste heat, resistive heater, natural gas heater, heat pump in heating mode) and three cooling methods (surface water, ambient air, heat pump in cooling mode) are considered. Reference values of τ_h and τ_c are reported in Table 1. These values are illustrative, selected to apply and showcase the outcome of the proposed methodology and, therefore, should not be regarded as prescriptive design data. It should be noted that, in perspective, the simultaneous use of a heat pump for both heating and cooling represents an interesting system-integration strategy. However, a rigorous evaluation of such dual-purpose operation would require a component-level or distributed model capable of resolving temperature levels, heat-exchanger effectiveness, and load matching, which is beyond the lumped-parameter framework adopted in this study.

Finally, while the above framework is energy-based, aggregating different energy carriers (thermal, electrical, solar) is not rigorous from a thermodynamic standpoint because of their differing exergy content. A fully consistent comparison across technologies would require an exergy analysis [23]. For this reason, in this work the contributions are deliberately kept disaggregated while acknowledging that an exergy-based approach would represent the logical next step.

3. Results and discussion

In this section, the results of the energetic analyses for the different system configurations are presented. For all three configurations, the energy requirements estimated on the basis of the thermodynamic model are reported in Section 3.1. These requirements depend exclusively on the system configuration and operating conditions and are independent of the technological solution adopted to supply or remove the corresponding energy flows. The impact of specific energy sources and of the technologies used to meet these requirements is subsequently addressed for a selected configuration in Section 3.4. There, an indicative estimate of the resulting energy consumption is presented for different heat source and heat sink scenarios, emphasizing the importance of thoroughly assessing the overall energy profile and the impact of resource availability.

Table 1
Reference τ values selected for the performed analysis. Values are indicative and used solely to demonstrate the methodology. Actual performance depends on technology, operating conditions, and local environmental conditions. Values should not be used as prescriptive design parameters.

Heating	Solar thermal	Waste heat	Resistive heater	Natural gas heater	Heat pump (heater)
τ_h (−)	0.65 ± 0.15	∞	0.95 ± 0.04	0.75 ± 0.10	4 ± 0.50

Cooling	Surface water	Ambient air	Heat pump (chiller)
τ_c (−)	∞	∞	3 ± 0.50

3.1. Thermodynamic behavior of MD systems

3.1.1. Configuration 1 – DCMD with open feed and closed distillate circuits

Fig. 3A) and D) present the performance maps for DCMD operated with the distillate side in closed circuit and the feed side in open circuit (configuration 1). The plots report the SCR (Fig. 3A) and the STEC (Fig. 3D) as functions of η (x-axis) and ΔT (y-axis). The colour scale represents the magnitude of each metric, while the black contour lines correspond to isovalues. Notice that both SCR and STEC are normalized with respect to the distillate production $\dot{m}_d$, which is dependent on both temperature variation in the feed channel (namely, $T_{h,in} - T_{h,out}$) and efficiency η. The white areas on the maps correspond to thermodynamically infeasible combinations of η and ΔT. As η increases, the admissible ΔT range shrinks progressively. In other words, once $\Delta T_{h,in}$ is fixed, not all combinations of recovery rate and temperature difference are simultaneously achievable, because they would violate either first-principal energy conservation, second-principal consistency (efficiency exceeding unity), or mass conservation (negative residual feed flow). The maps thus visually encode the operational feasibility boundaries of DCMD, set jointly by the first and second laws of thermodynamics and by the mass conservation of the feed stream.

For SCR (Eq. (1)) the isolines appear nearly vertical, particularly at low efficiencies, because the increase in productivity ($\dot{m}_d$) related with increasing ΔT is of similar magnitude with respect to the temperature increase experienced by the distillate stream. As a result, SCR is dominated by the $1/\eta$ dependence: it decreases with increasing efficiency, while its sensitivity to ΔT remains limited. Put differently, the cooling duty per unit of freshwater produced is nearly invariant with respect to ΔT: for each unit of energy transferred from the feed stream to the distillate stream within the module, an almost equivalent amount must be extracted on the cooling side. Again, this is valid when a constant $\Delta T_{h,in}$ is considered. By contrast, STEC (Eq. (1)) exhibits isolines with a

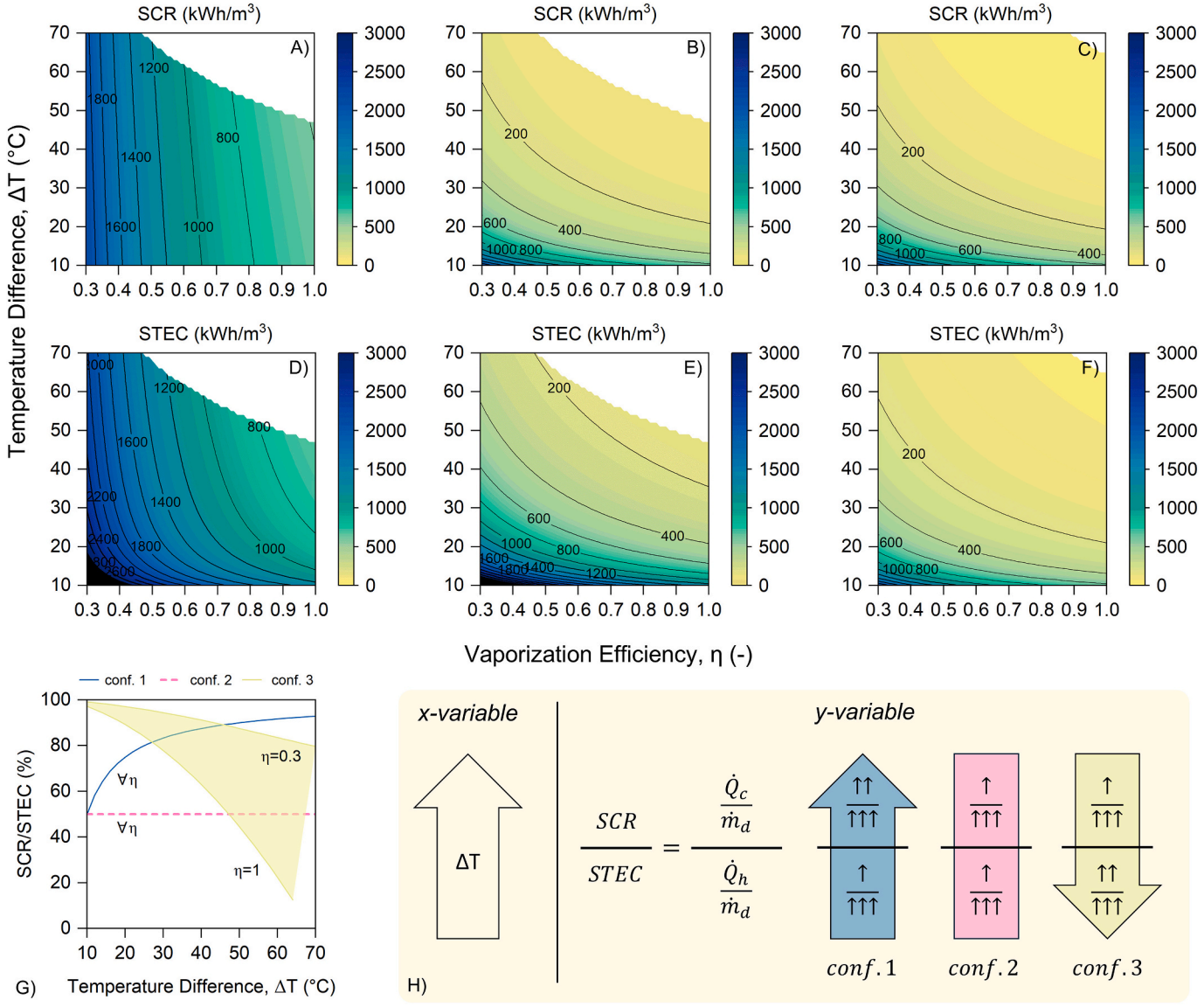

Fig. 3. Cooling and heating requirements for the three investigated MD configurations. Panels A), B) and C) (first row) report the specific cooling requirement (SCR), i.e., the energy that must be removed per cubic meter of produced distillate, for configuration 1, configuration 2, and configuration 3, respectively. Panels D), E) and F) (second row) show, for comparison, the specific thermal energy consumption (STEC) of the same configurations. All filled contour maps are plotted as functions of the independent variables η (x-axis) and ΔT (y-axis). Panel G) reports the SCR /STEC ratio against ΔT, quantifying the relative impact of cooling over heating: a value of 100% indicates equal contributions. The shaded green band in panel G) represents the variability associated with η in configuration 3, in which the ratio depends on $\Delta T_{h,out}$ and in cascade on η (Eqs. S14 and S15). Panel H) schematically rationalizes the trend observed in G), illustrating how increasing ΔT influences both SCR and STEC.

hyperbolic shape. At high ΔT values (above 50 °C, where $\Delta T \gg \Delta T_{h,out}$) and low η the contours are nearly vertical, but moving to lower ΔT and higher efficiencies they progressively flatten. STEC remains systematically higher than SCR in the open feed configuration: the heating duty must not only replenish the enthalpy drop of the feed stream across the module (from $T_{h,out}$ to $T_{h,in}$) and sustain vaporization, but must also compensate for the sensible enthalpy that irreversibly leaves the system with the feed effluent stream. Since the feed is not recirculated, all this sensible energy must be replenished at every cycle, amplifying the heating demand (i.e., power required to continuously raise the feed stream temperature from $T_{ambient}$ to $T_{h,in}$) and increasing the nonlinear dependence on ΔT. Overall, configuration 1 demonstrates that cooling and heating duties are in this case thermodynamically asymmetric.

3.1.2. Configuration 2 – DCMD with external heat recovery

In this configuration, the DCMD module is coupled with an external heat exchanger that recovers the heat released by the distillate stream to pre-heat the feed before it enters the module. The feed and distillate circuits remain open and closed, respectively. For simplicity, a temperature difference of $\Delta T_{HX} = 5$ °C is imposed across the heat exchanger, assuming it to be constant along the heat exchanger length. Assuming a different ΔT_{HX} would change the absolute SCR and STEC values, and therefore their ratio, but not the overall trends and outcomes. In this configuration, the cooling duty corresponds therefore to the removal of the constant temperature difference across the heat exchanger from distillate stream (namely, $T_3 - T_{c,in} = T_3 - T_1 = \Delta T_{HX}$, see Fig. S3B)). Consequently, the active cooling requirement is capped and no longer scales with the full distillate side temperature rise observed in configuration 1. On the heating side, the duty now corresponds to raising the feed temperature by $\Delta T_{h,in} + \Delta T_{HX}$, i.e., the intrinsic temperature lift $\Delta T_{h,in}$ plus the additional pinch imposed by the heat exchanger (namely, $T_{h,in} - T_2 = T_{h,in} - (T_{c,out} - \Delta T_{HX}) = \Delta T_{h,in} + \Delta T_{HX}$), see Fig. S3B)). Fig. 3B) and E) show the corresponding SCR and STEC maps. The metrics exhibit isocontours of similar shape, being proportional to a constant (namely, ΔT_{HX} and $\Delta T_{h,in} + \Delta T_{HX}$, for SCR and STEC, respectively) and $1/(\eta(\Delta T - \Delta T_{h,out}))$. Their absolute levels differ: SCR is limited by the fixed ΔT_{HX}, while *STEC* is shifted upward by the additional $\Delta T_{h,in}$ contribution. At low efficiencies (η = 0.3–0.4), both metrics decrease steeply with increasing η, reflecting the dominant $1/\eta$ dependence. As efficiency approaches unity, contour lines approach an asymptotic plateau. Then, higher ΔT leads to a consistent reduction in both SCR and STEC. Thermodynamically, the key difference from configuration 1 is that the full distillate side enthalpy gain is now largely recycled into the feed stream via the heat exchanger, reducing both heating and cooling loads to fixed and internally balanced values. This configuration stabilizes the energy balance and reduces the dependence on external utilities. Overall, configuration 2 highlights the thermodynamic advantage of integrating heat recovery in DCMD.

3.1.3. Configuration 3 – closed-circuit AGMD with internal heat recovery

The third configuration employs an AGMD module with internal heat recovery. The distillate condenses into the gap, while the same saltwater stream circulates through both hot and cold channels, forming a closed circuit. After exiting the hot side, the stream is cooled to $T_{c,in}$ and a mass flow rate equal to the distillate produced in a single pass ($\dot{m}_d$) is reintroduced to enable pseudo-steady-state conditions. Before re-entering the hot channel, the stream is heated to the hot inlet temperature setpoint $T_{h,in}$. Fig. 3C) and F) report contour plots of SCR and *STEC*: both metrics share the same functional dependence on η *and* ΔT, differing only in their scaling factors. With $\Delta T_{h,in}$ fixed at 5 °C, *STEC* is simply scaled by this constant, while SCR depends on $\Delta T_{h,out}$, which is slightly smaller because of the recovery rate. As a result, *STEC* values are systematically higher, consistent with $\Delta T_{h,in} > \Delta T_{h,out}$. The closed-circuit configuration couples heating and cooling within the same stream, producing nearly parallel contour maps and minimizing external utility needs. Configuration 3 therefore illustrates the intrinsic thermodynamic balance of AGMD, where internal energy recycling redistributes enthalpy flows and sharply reduces external heating and cooling requirements.

3.1.4. Practical implications and scalability considerations

The thermodynamic maps of Fig. 3 reveal the fundamental behavior of the three MD configurations. Since fixing $\Delta T_{h,in}$ at 5 °C implies considering modules of different sizes, comparing different points of each panel corresponds to operating different modules. In other words, moving across isocontours does not simulate the operation of a single device under varying conditions, but rather compares distinct systems designed to satisfy the imposed boundary constraints. For instance, considering a larger ΔT while maintaining the same conditions ($\Delta T_{h,in}$, fluid dynamics, module characteristics) necessarily requires a longer module or module train, as the module length directly influences the terminal temperature differences. Alternatively, achieving smaller or larger terminal temperature differences (at the module inlet and outlet), while keeping the same overall ΔT, inherently requires a longer or shorter module, respectively [24–26]. In fact, operating laboratory-scale units, where the feed exits at relatively high temperature and the distillate at relatively low temperature, naturally yield to higher terminal temperature differences compared to pilot or full-scale systems when the inlet temperatures are fixed [27]. Accordingly, the results presented herein apply to systems designed in accordance with the assumptions adopted in this study. They are therefore not restricted to laboratory or pilot-scale setups, but extend to any system that satisfies the same design conditions.

From a techno-economic perspective, a clear trade-off emerges between capital and operating costs. Reducing specific energy requirements relies on efficient heat utilization, achieved by combining larger modules, which minimize terminal temperature differences while increasing active area, with designs exploiting heat recovery. Such highly optimized systems may achieve lower STEC and SCR but entail high capital investment, whereas compact units minimize CapEx but suffer from disproportionately high OpEx [24]. This scaling behavior identifies a thermodynamic–economic frontier for MD: reductions in energy requirements are constrained by consequential increase in heat transfer areas and pumping demands [24]. More broadly, this frontier exemplifies a universal design constraint in low-grade heat utilization systems, where supply temperature reduction is constrained by surface-driven energy transfer and hydraulic resistance [28,29].

3.2. The role of cooling on overall thermal energy flows

Fig. 3G) compares the SCR/*STEC* ratio, which quantifies the relative impact of cooling over heating. A value of 100% indicates that cooling and heating contribute equally to the overall energy balance. The ratio is reported as a function of ΔT and η. To rationalize the trends shown, a schematic representation of ΔT influence on the SCR/*STEC* ratio is reported in Fig. 3H). For configuration 1, the SCR/*STEC* ratio increases with ΔT, and approaches unity at high ΔT values, showing that cooling can become nearly as significant as heating. This trend underscores that, in conventional DCMD systems, cooling duties cannot be neglected, especially at high temperature differences. In configuration 2, the SCR/*STEC* ratio is constant and independent of ΔT. In the present analysis, the ratio stabilizes at 50%. By design, the cooling and heating contributions are locked into a fixed proportion, and ΔT no longer alters their balance. Moving to configuration 3, SCR/*STEC* depends directly on the $\Delta T_{h,out}/\Delta T_{h,in}$ ratio. Its value is not fixed, but depends on single-pass water recovery and, consequently, on vaporization efficiency. The only imposed physical constraint is that $\Delta T_{h,out} \geq 0.5$ °C to ensure a finite driving force for heat transfer. As a result, the SCR/STEC ratio is represented by a shaded band, bound by the limits corresponding to η = 0.3 and $\eta = 1$. For small ΔT values (around 10 °C), the recovery is low, the heat capacities of the hot and cold streams are nearly equal, and the MD module behaves almost like a simple heat exchanger with negligible

mass transfer (i.e., vapor generation). In this regime, SCR/STEC → 1. As ΔT increases, $\Delta T_{h,out}$ approaches its lower threshold (0.5 °C, with $\Delta T_{h,in}$ = 5 °C fixed), causing the SCR/STEC ratio to decrease accordingly.

Overall, this analysis shows that cooling loads, often neglected in MD studies, can approach or even match heating requirements, depending on system configuration and operating conditions. The way cooling is managed, either dissipated externally or recycled internally, significantly shapes the energy footprint of MD systems, underlining the need to account for cooling explicitly in both design and operational assessment.

3.3. Thermodynamic implications of single-pass water recovery and pumping energy

Fig. 4 summarizes, taking configuration 3 as the baseline, the variation of single-pass water recovery and of the pumping energy required to circulate water within the module as functions of η and ΔT. Panel A) reports a general sketch of what is meant by single-pass water recovery. Panel B) shows instead iso-ΔT curves (10–70 °C) for the recovery rate as a function of η. With an imposed $\Delta T_{h,in}$, an increase in ΔT implies a longer module length and thus a larger active area. As a result, recovery increases with increasing temperature difference, yet it remains thermodynamically bound by the imposed inlet temperature difference $\Delta T_{h,in}$ = 5 °C and by the minimum achievable $\Delta T_{h,out}$ (0.5 °C) (Eq. S8). The maximum single-pass water recovery R observed at the largest ΔT (achieved for η lower than 0.9) arises from a fundamental thermodynamic and mass balance limitation. Achieving such recoveries would require conditions that are incompatible with the boundary conditions adopted in this study. Moreover, larger ΔT shift energy use from vaporization (latent) to sensible heat, which effectively limits the maximum achievable recovery rate. This behavior highlights the interplay between temperature driving forces, module exit conditions, and the partitioning of energy between sensible and latent heat in single-pass MD systems.

Panel C) reports the corresponding pumping energy per cubic meter of produced water, considering three different hydraulic pressure losses scenarios across the MD module (100, 300, and 1000 mbar). Specific pumping energy consumption decreases monotonically with increasing η because less feed water must circulate per unit of produced distillate. To facilitate a direct comparison between energy and recovery, four representative operating points are highlighted with gray triangular markers in Panels B) and C). At η = 0.5, the corresponding recoveries are only 2.2% and 3.9% for ΔT = 30 °C and 50 °C, respectively. At higher efficiency (η = 0.7), the recoveries rise to 3.0% and 5.6%. Larger ΔT lowers the pumping penalty by increasing the single-pass water recovery, while higher pressure losses shift all curves upwards, demonstrating the direct contribution of hydraulic resistance to the energy footprint.

Overall, pumping energy, although often downplayed in MD studies, can constitute a significant contribution to the total energy requirements of the system. Although its absolute values in kWh/m^3 are significantly lower than those associated with heating and cooling, as shown in Figs. 3 and 4, pumping requires energy with high exergy content. For this reason, its contribution cannot be regarded as negligible. These observations underscore the importance of integrated design strategies that jointly consider thermal driving forces, recovery targets, and hydraulic optimization to minimize the overall energy footprint of membrane distillation systems.

3.4. The gap between theoretical analyses and real systems

To illustrate practical implications, the framework presented in Section 2.3 is applied to configuration 3, representing the most advanced configuration currently available [30]. Under realistic operating conditions (η and ΔT equal to respectively 0.7 and 40 °C), STEC and SCR values of respectively 129 kWh/m^3 and 98 kWh/m^3 are obtained. Fig. 5 compares the specific energy consumption $\dot{w}$, and its corresponding net value, $\dot{w}_{net}$, for different heating and cooling options. Horizontal lines mark the baseline STEC and SCR values, highlighting the discrepancy between theoretical requirements and necessary real energy inputs, once the device conversion factors presented in Table 1 (τ_h, τ_c) are considered. The patterned portion of the bars quantifies the energy consumption for auxiliary technical streams circulation ($\dot{w}_{pump}$). Note that such pumping contributions are associated with heating and cooling activities and thus differ from the pumping requirements for streams circulation within the MD module. The constant values assumed here are meant solely as order-of-magnitude estimates and should not be interpreted as blueprints or reference values.

Several insights emerge. Solar and waste heat offer the lowest net consumption (k_2 = 0), while paid energy carriers exceed the nominal STEC values because of conversion losses. Heat pumps enable to reduce both total and net consumptions when temperature levels are favorable, owing to COP values >1, but this comes at the price of increased electrification and capital costs. For cooling, surface water and ambient air are cost-effective sinks, while chillers impose steep electrical penalties. With reference to the conditions mentioned above, the thermodynamic cooling-to-heating ratio (SCR/STEC ≈ 76%) can translate into vastly different operating-cost ratios depending on heat sources and heat sinks availability. As an example, exploiting surface water for cooling will not

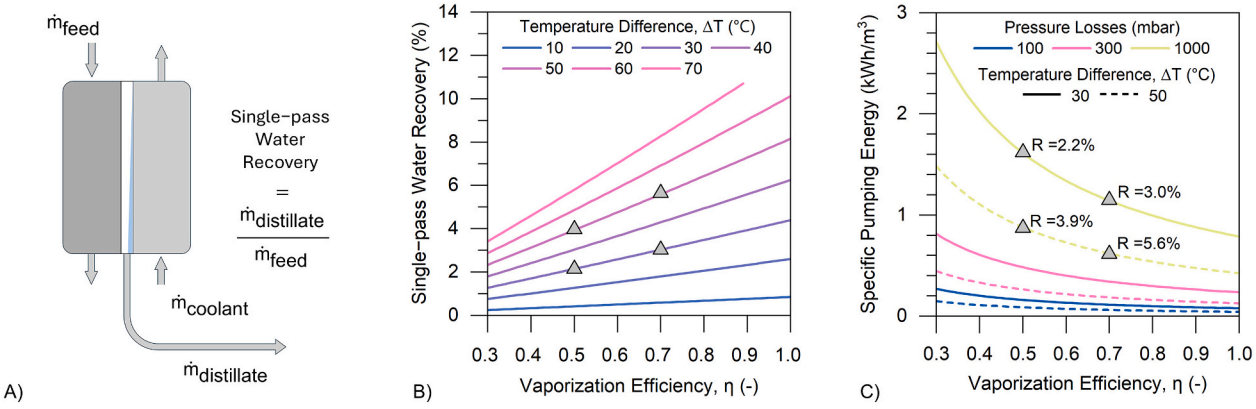

Fig. 4. Single-pass water recovery and its impact on specific pumping energy requirements are analyzed for the AGMD configuration, taken here as a representative case. Panel A) illustrates the concept of single-pass recovery while panel B) displays how the single-pass water recovery varies with η (x-axis) and ΔT (colour scale). Panel C) reports the pumping energy required per cubic meter of produced distillate as a function of η (x-axis), assuming three different hydraulic pressure losses across the MD module (colour-coded). For each pressure level, two curves are shown, corresponding to ΔT values of 30 °C and 50 °C, respectively. The presence of paired curves reflects that specific pumping energy depends on the water recovery, which in turn is dependent on both η and ΔT.

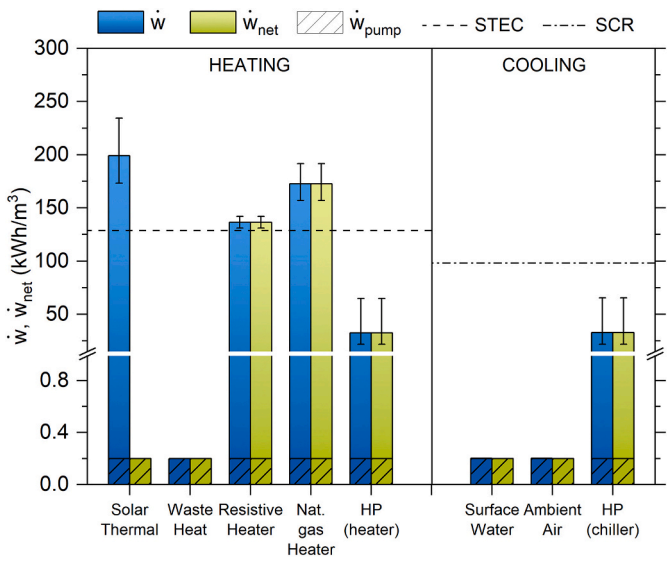

Fig. 5. Specific energy consumptions for configuration 3. Blue bars ($\dot{w}$) indicate the total consumptions of each heating/cooling option, while green bars ($\dot{w}_{net}$) show the corresponding net consumptions once freely available sources are accounted for. The patterned portions of the bars quantify the contribution of auxiliary pumping ($\dot{w}_{pump}$), which is arbitrarily selected here for simplicity. Horizontal lines correspond to the baseline STEC and SCR values, i.e., the theoretical heating and cooling requirements per cubic meter of produced distillate water, highlighting the gap between thermodynamic requirements and real system energy consumptions. A y-axis break from 1 to 10 kWh/m^3 is introduced to better visualize the trends.

affect SCR nor STEC, however it drives the ratio cooling/heating of operating costs ($\dot{w}_{c,net}/\dot{w}_{h,net}$) towards values approaching 0. More interestingly, using waste heat without a viable sink can raise the ratio up to 20,000% ($\dot{w}_{c,net} \approx 40$ kWh/m^3 and $\dot{w}_{h,net} \approx 0.2$ kWh/m^3), unveiling the need to evaluate heating and cooling jointly.

These results depend strongly on local conditions, such as heat source/heat sink temperatures, available flow rates, ambient temperatures and consequent COP values, and should be evaluated through case-specific analyses. While heat pumps could, under reasonable assumptions (COP 3 for cooling and COP 4 for heating [31]), push the total energy consumption below the theoretical requirements, they significantly increase both capital costs and electrical dependency, undermining MD's advantage as a low-grade-energy technology. In general, however, the electrification of heat sources and heat sinks is not an issue specific to MD alone. This consideration applies more broadly to thermal desalination technologies, including multi-effect distillation, multi-stage flash, humidification dehumidification desalination, and generic desalination processes that are driven by thermal energy, since the origin of the heat source governs not only the intrinsic energy consumption of the process but also its overall sustainability. In addition, also the thermodynamic imbalance between heating and cooling uncovered here goes well beyond MD. It points to a broader limitation shared by all technologies trying to make use of low-grade heat for separation or purification: without an adequate heat sink, even "free" thermal energy cannot be used effectively. This changes how the utilization of waste heat in energy–water systems should be approached. Instead of focusing only on where heat can be found, future designs need to consider how that heat can also be released and managed. MD is, in this sense, a model case for exploring the true limits of waste heat recovery. Its implications extend to all systems where temperature differences are small and thermal irreversibility high, such as carbon capture, where the same thermodynamic asymmetry governs solvent regeneration and reabsorption, and industrial resource recovery, where it governs evaporative concentration and condensation cycles.

4. Conclusion

The present analysis was intended to clarify the thermodynamic positioning and system-level implications of operating a membrane distillation system. The proposed framework should be regarded as a rapid screening and conceptual design tool. The results are applicable at the system scale and are intended to serve as guidelines to identify trends and to highlight the importance of a holistic approach when designing MD systems. Under typical conditions, cooling loads can reach the same magnitude as heating, making the availability of adequate heat sinks a defining constraint. Integrating external heat recovery stabilizes this ratio (around 50% for a 5 °C exchanger pinch) but cannot eliminate the underlying thermal burden, whereas exploiting internal heat recovery may drive the SCR/STEC ratio towards lower values. Circulating the feed stream adds 0.2–0.5 kWh/m^3 for hydraulic losses of 100–300 mbar, a significant fraction considering the low single-pass water recoveries (2–6%) typical of the MD technology. In addition, a methodology is proposed to translate theoretical energy requirement values into estimates of actual system energy consumption. This approach enables the evaluation of the impact of different heating and cooling technologies, as well as the potential benefits associated with the use of available heat sources and heat sinks.

Overall, the results point out that membrane distillation is not only limited by heating requirements, but also by cooling and pumping demands, which may be considered in terms of their associated energy and exergy loads. "Free" heat alone does not guarantee viability: successful deployment demands matched heat sinks, rational recovery design, and low-resistance module hydraulics. Unless these thermal and hydraulic constraints are co-optimized at system level, MD will remain a thermodynamic curiosity rather than a scalable desalination route.

CRediT authorship contribution statement

Marco Malaguti: Conceptualization, Formal analysis, Investigation, Methodology, Visualization, Software, Writing – original draft, Writing – review & editing. **Matteo Morciano:** Formal analysis, Investigation, Methodology, Visualization, Validation, Writing – original draft, Writing – review & editing. **Giulia Viano:** Formal analysis, Investigation, Methodology, Software, Writing – review & editing. **Andrea Achilli:** Conceptualization, Writing – review & editing. **Aamer Ali:** Validation, Funding acquisition, Resources, Writing – review & editing. **Cejna Anna Quist-Jensen:** Validation, Funding acquisition, Resources, Writing – review & editing. **Alberto Tiraferri:** Conceptualization, Supervision, Writing – original draft, Writing – review & editing.

Declaration of competing interest

The authors declare that they have no known competing financial interests or personal relationships that could have appeared to influence the work reported in this paper.

Acknowledgments

This work was funded by the European Union Horizon Europe Research and Innovation Programme under grant agreement number 101091915 (acronym "MEloDIZER"). Views and opinions expressed are however those of the author(s) only and do not necessarily reflect those of the European Union or the European Health and Digital Executive Agency (HADEA). Neither the European Union nor the granting authority can be held responsible for them.

Appendix A. Supplementary data

Supplementary data to this article can be found online at https://doi.org/10.1016/j.desal.2026.120039.

Data availability

All data generated during this study are included in this published article and its supplementary information file.

References

[1] V.G. Gude, Desalination and sustainability – an appraisal and current perspective, Water Res. 89 (Feb. 2016) 87–106, https://doi.org/10.1016/j.watres.2015.11.012.

[2] M. Di Vincenzo, et al., 2-Hydroxy-N-(diphenylmethyl) acetamide nanocomposite membranes for highly selective desalination, J. Membr. Sci. 721 (Apr. 2025) 123785, https://doi.org/10.1016/j.memsci.2025.123785.

[3] H. Saboori, H. Mehrjerdi, Tri-objective optimization of a synergistic wind-photovoltaic plant for water desalination addressing sustainable development goals, Sustain. Dev. 30 (6) (Dec. 2022) 1811–1822, https://doi.org/10.1002/sd.2349.

[4] A.M. Hamiche, A.B. Stambouli, S. Flazi, A review of the water-energy nexus, Renew. Sust. Energ. Rev. 65 (Nov. 2016) 319–331, https://doi.org/10.1016/j.rser.2016.07.020.

[5] A. Deshmukh, et al., Membrane distillation at the water-energy nexus: limits, opportunities, and challenges, Energy Environ. Sci. 11 (5) (2018) 1177–1196, https://doi.org/10.1039/C8EE00291F.

[6] M. Malaguti, L.K. Presson, A. Tiraferri, K.L. Hickenbottom, A. Achilli, Productivity, selectivity, and energy consumption of pilot-scale vacuum assisted air-gap membrane distillation for the desalination of high-salinity streams, Desalination 582 (Aug. 2024) 117511, https://doi.org/10.1016/j.desal.2024.117511.

[7] R.R. Meo, et al., Systematic exploration of direct solar absorption potential to enhance direct contact membrane distillation, Desalination 606 (Jul. 2025) 118740, https://doi.org/10.1016/j.desal.2025.118740.

[8] R. Ullah, et al., Energy efficiency of direct contact membrane distillation, Desalination 433 (May 2018) 56–67, https://doi.org/10.1016/j.desal.2018.01.025.

[9] F.E. Ahmed, B.S. Lalia, R. Hashaikeh, N. Hilal, Alternative heating techniques in membrane distillation: a review, Desalination 496 (Dec. 2020) 114713, https://doi.org/10.1016/j.desal.2020.114713.

[10] M. Khayet, Solar desalination by membrane distillation: dispersion in energy consumption analysis and water production costs (a review), Desalination 308 (Jan. 2013) 89–101, https://doi.org/10.1016/j.desal.2012.07.010.

[11] H.C. Duong, P. Cooper, B. Nelemans, T.Y. Cath, L.D. Nghiem, Evaluating energy consumption of air gap membrane distillation for seawater desalination at pilot scale level, Sep. Purif. Technol. 166 (Jun. 2016) 55–62, https://doi.org/10.1016/j.seppur.2016.04.014.

[12] J.J. Peguero-Pina, A. Vilagrosa, D. Alonso-Forn, J.P. Ferrio, D. Sancho-Knapik, E. Gil-Pelegrín, Living in drylands: functional adaptations of trees and shrubs to cope with high temperatures and water scarcity, Forests 11 (10) (Sep. 2020) 1028, https://doi.org/10.3390/f11101028.

[13] K. Eisenack, Institutional adaptation to cooling water scarcity for thermoelectric power generation under global warming, Ecol. Econ. 124 (Apr. 2016) 153–163, https://doi.org/10.1016/j.ecolecon.2016.01.016.

[14] P. Rajala, M. Bomberg, E. Huttunen-Saarivirta, O. Priha, M. Tausa, L. Carpén, Influence of chlorination and choice of materials on fouling in cooling water system under brackish seawater conditions, Materials 9 (6) (Jun. 2016) 475, https://doi.org/10.3390/ma9060475.

[15] W.-Y. Qi, Y.-W. Wei, Z. Wang, S.-C. Gong, C. Song, S.-G. Wang, Does the concentration ratio contribute to the scaling of circulating cooling seawater? Desalination 576 (May 2024) 117347 https://doi.org/10.1016/j.desal.2024.117347.

[16] J. Swaminathan, H.W. Chung, D.M. Warsinger, J.H. Lienhard V, Membrane distillation model based on heat exchanger theory and configuration comparison, Appl. Energy 184 (Dec. 2016) 491–505, https://doi.org/10.1016/j.apenergy.2016.09.090.

[17] F. Signorato, M. Morciano, L. Bergamasco, M. Fasano, P. Asinari, Exergy analysis of solar desalination systems based on passive multi-effect membrane distillation, Energy Rep. 6 (Nov. 2020) 445–454, https://doi.org/10.1016/j.egyr.2020.02.005.

[18] H. Zhang, S. Shao, H. Xu, H. Zou, C. Tian, Free cooling of data centers: a review, Renew. Sust. Energ. Rev. 35 (Jul. 2014) 171–182, https://doi.org/10.1016/j.rser.2014.04.017.

[19] R.R. Meo, et al., Systematic exploration of direct solar absorption potential to enhance direct contact membrane distillation, Desalination 606 (Jul. 2025) 118740, https://doi.org/10.1016/j.desal.2025.118740.

[20] K.S.S. Christie, T. Horseman, S. Lin, Energy efficiency of membrane distillation: simplified analysis, heat recovery, and the use of waste-heat, Environ. Int. 138 (May 2020) 105588, https://doi.org/10.1016/j.envint.2020.105588.

[21] M. Giagnorio, M. Morciano, W. Zhang, C. Hélix-Nielsen, M. Fasano, A. Tiraferri, Coupling of forward osmosis with desalination technologies: system-scale analysis at the water-energy nexus, Desalination 543 (Dec. 2022) 116083, https://doi.org/10.1016/j.desal.2022.116083.

[22] M.H. Sharqawy, J.H. Lienhard, S.M. Zubair, Thermophysical properties of seawater: a review of existing correlations and data, Desalin. Water Treat. 16 (1–3) (Apr. 2010) 354–380, https://doi.org/10.5004/dwt.2010.1079.

[23] T. Altmann, J. Robert, A. Bouma, J. Swaminathan, J.H. Lienhard, Primary energy and exergy of desalination technologies in a power-water cogeneration scheme, Appl. Energy 252 (Oct. 2019) 113319, https://doi.org/10.1016/j.apenergy.2019.113319.

[24] J. Swaminathan, H.W. Chung, D.M. Warsinger, J.H. Lienhard V, Membrane distillation model based on heat exchanger theory and configuration comparison, Appl. Energy 184 (Dec. 2016) 491–505, https://doi.org/10.1016/j.apenergy.2016.09.090.

[25] M. Hardikar, I. Marquez, A. Achilli, Emerging investigator series: membrane distillation and high salinity: analysis and implications, Environ. Sci.: Water Res. Technol. 6 (6) (2020) 1538–1552, https://doi.org/10.1039/C9EW01055F.

[26] J. Swaminathan, H.W. Chung, D.M. Warsinger, J.H. Lienhard V, Energy efficiency of membrane distillation up to high salinity: evaluating critical system size and optimal membrane thickness, Appl. Energy 211 (Feb. 2018) 715–734, https://doi.org/10.1016/j.apenergy.2017.11.043.

[27] M. Hardikar, I. Marquez, T. Phakdon, A.E. Sáez, A. Achilli, Scale-up of membrane distillation systems using bench-scale data, Desalination 530 (May 2022) 115654, https://doi.org/10.1016/j.desal.2022.115654.

[28] M. Capone, E. Guelpa, V. Verda, Potential for supply temperature reduction of existing district heating substations, Energy 285 (Dec. 2023) 128597, https://doi.org/10.1016/j.energy.2023.128597.

[29] J. Hu, S. Fan, B. Zhang, C. He, Z. Liu, Q. Chen, Optimal design of heat pump integrated low-grade heat utilization systems, Energy Convers. Manag. 260 (May 2022) 115619, https://doi.org/10.1016/j.enconman.2022.115619.

[30] J.A. Andrés-Mañas, J.D. Gil, J.A. Sánchez-Molina, M. Berenguel, G. Zaragoza, Operation, control and assessment of a full-scale membrane distillation unit for treating desalination brine in the context of greenhouse production, J. Clean. Prod. 503 (Apr. 2025) 145186, https://doi.org/10.1016/j.jclepro.2025.145186.

[31] K. Pérez, S. Díaz-Quezada, D. Zamora, H. Estay, Heat pump assisted air gap and direct contact membrane distillation configurations: comparative simulations of industrial scale cases at the water-energy nexus, Energy 315 (Jan. 2025) 134369, https://doi.org/10.1016/j.energy.2025.134369.